Response to Liu Mingliang

essd-2023-495

Title: Satellite-based Near-Real-Time Global Daily Terrestrial Evapotranspiration Estimates

Author(s): Lei Huang et al.

MS type: Data description paper

In the reply, the reviewers' comments are in *italics*, our response is in normal text, and quotes from the manuscript are in **blue**.

I still doubt the advantage of this study from other earlier data products. The authors claim that this new products can estimate ET in within a week rather than other products delays of more than two weeks (L617-619), while this new data product is not near-real time at all (only covers 2001-2022) and there is no operational platform provides this (near-real time) service. The descriptions on the equations are still confusing in many places (the organization of equations in the text and appendix need rearrangement). Some equation numbers in Fig 1 are wrong. The comparisons (and evaluations) between ET products from this study and GPCC precipitation is not direct and no robust conclusions could produced from this comparison (although authors claim that there are matched spatial pattern as described in L730-734, other models or products could have the same results). This paper did a good job in comparing this data products with others and observations from fluxnet, while it could do a better job to fix the problems (i.e. decrease the biases) since the method itself (VISEA) had already been developed well before this paper.

Re: we thank the reviewers!

We have updated our ET data product up to March 20, 2024. All current data can be accessed online at https://doi.org/10.11888/Terre.tpdc.300782. We are committed to continuously updating this dataset, ensuring that the latest ET data will be consistently and promptly made available. Further, we have included a description of the operational platform that supports this dataset at lines 735-740:

The VISEA code for calculating daily ET is written in C and can be executed on Windows 10 using an Intel(R) Core (TM) i7-8565U CPU @ 1.80GHz, 1.99 GHz, 16.0 GB RAM with Visual Studio 2019, or compatible platforms. Additionally, it can run on high-performance computing servers equipped with an Intel(R) Xeon(R) CPU E5-2680 in a CentOS environment. The system is scalable, supporting configurations ranging from 20 nodes and 656 CPUs down to fewer nodes and CPUs as required.

We have reorganized and clarified the descriptions of equations within the text and appendix. These changes can be found at lines 141-178:

2.1.1 Daily evaporation fraction calculation

Combining Eq. 1, 2 and 3, we calculated the instantaneous evaporation fraction, $\boldsymbol{EF^i}$ as:

$$EF^i = f_{veg}\frac{Q^i_{veg}}{Q^i}\,EF^i_{veg} + (1 - f_{veg})\frac{Q^i_{soil}}{Q^i}\,EF^i_{soil} \quad (4)$$

EF^i_{veg} and EF^i_{soil} are the instantaneous full vegetation coverage and bare soil EF, respectively. EF^i_{veg} can be expressed as a function of instantaneous parameters (Nishida et al., 2003):

$$EF^i_{veg} = \frac{\alpha\,\Delta^i}{\Delta^i + \gamma(1 + r^i_{c\,veg}/2r^i_{a\,veg})} \quad (5)$$

where α is the Priestley-Taylor parameter, which was set to 1.26 for wet surfaces (De Bruin, 1983); Δ^i is the instantaneous slope of the saturated vapor pressure, which is a function of the temperature (Pa K^{-1}); γ is the psychometric constant (Pa K^{-1}); $r^i_{c\,veg}$ is the instantaneous surface resistance of the vegetation canopy (s m^{-1}); $r^i_{a\,veg}$ is the instantaneous aerodynamics resistance of the vegetation canopy (s m^{-1}). EF^i_{soil} was expressed by Nishida et al. (2003) as a function of the instantaneous soil temperature and the available energy based on the energy budget of the bare soil:

$$EF^i_{soil} = \frac{T^i_{soil\,max} - T^i_{soil}}{T^i_{soil\,max} - T^i_a}\frac{Q^i_{soil0}}{Q^i_{soil}} \quad (6)$$

where $T^i_{soil\,max}$ is the instantaneous maximum possible temperature at the surface reached when the land surface is dry (K), T^i_{soil} is the instantaneous temperature of the bare soil (K), T^i_a is the instantaneous air temperature, Q^i_{soil0} is the instantaneous available energy for bare soil when T^i_{soil} is equal to T^i_a (W m^{-2}).

As the assumption of noon time instantaneous evaporation fraction EF^i equals daily average evaporation fraction, EF^d, thus, $EF^i = EF^d$, caused a 10%-30% underestimation of daily ET (Huang et al., 2017; Yang et al., 2013), we introduced a decoupling parameter to covert EF^i into EF^d (Huang et al., 2021; Tang et al., 2017; Tang and Li, 2017). The superscript "d" means daily and "i" means instantaneous. This new decoupling parameter-based evaporation faction is developed from Penman-Monteith and McNaughton-Jarvis mathematical equations:

$$EF^d = EF^i\frac{\Delta^d}{\Delta^d + \gamma}\frac{\Delta^i + \gamma}{\Delta^i}\frac{\Omega^{*i}}{\Omega^{*d}}\frac{\Omega^d}{\Omega^i} \quad (7)$$

where Ω is the decoupling factor that represents the relative contribution of radiative and aerodynamic terms to the overall evapotranspiration (Tang and Li, 2017), Ω^*_i is the value of the decoupling factor, Ω, for wet surfaces. According to Pereira (2004), the calculation details of Ω and Ω^* are presented in Appendix B.

For full vegetation-covered areas, the decoupling parameter based daily EF^d_{veg} is expressed as:

$$EF_{veg}^{d} = \frac{\alpha\,\Delta^{i}}{\Delta^{i}+\gamma\left(1+\frac{r_{c\,veg}^{i}}{2r_{a\,veg}^{i}}\right)}\left(\frac{\Delta^{d}}{\Delta^{d}+\gamma}\frac{\Delta^{i}+\gamma}{\Delta^{i}}\frac{\Omega_{veg}^{*\,i}}{\Omega_{veg}^{*\,d}}\frac{\Omega_{veg}^{d}}{\Omega_{veg}^{i}}\right) \quad (8)$$

where $r_{c\,veg}^{i}$ is the instantaneous canopy resistance (s m^{-1}), $r_{a\,veg}^{i}$ is the instantaneous aerodynamic resistance (s m^{-1}). Determining these resistances are presented in Appendix C. For bare soil, the decoupling parameter based daily EF_{soil}^{d} is calculated as:

$$EF_{soil}^{d} = \frac{T_{soil\,max}^{\,i} - T_{soil}^{i}}{T_{soil\,max}^{\,i} - T_{a}^{i}}\frac{Q_{soil\,0}^{i}}{Q_{soil}^{i}}\left(\frac{\Delta^{d}}{\Delta^{d}+\gamma}\frac{\Delta^{i}+\gamma}{\Delta^{i}}\frac{\Omega_{soil}^{*\,i}}{\Omega_{soil}^{*\,d}}\frac{\Omega_{soil}^{d}}{\Omega_{soil}^{i}}\right) \quad (9)$$

Thus, EF^{d} is expressed as:

$$EF^{d} = f_{veg}\frac{Q_{veg}^{i}}{Q^{i}}\,EF_{veg}^{d} + (1-f_{veg})\frac{Q_{soil}^{i}}{Q^{i}}\,EF_{soil}^{d} \quad (10)$$

The same energy balance equations are used for calculating both instantaneous values Q^{i}, Q_{veg}^{i} and Q_{soil}^{i} and daily values Q^{d}, Q_{veg}^{d} and Q_{soil}^{d} but with parameters adjusted for each timeframe. The details of the calculation for the daily values are outlined below.

We have corrected the equation numbers in Figure 1 to ensure accuracy and clarity.

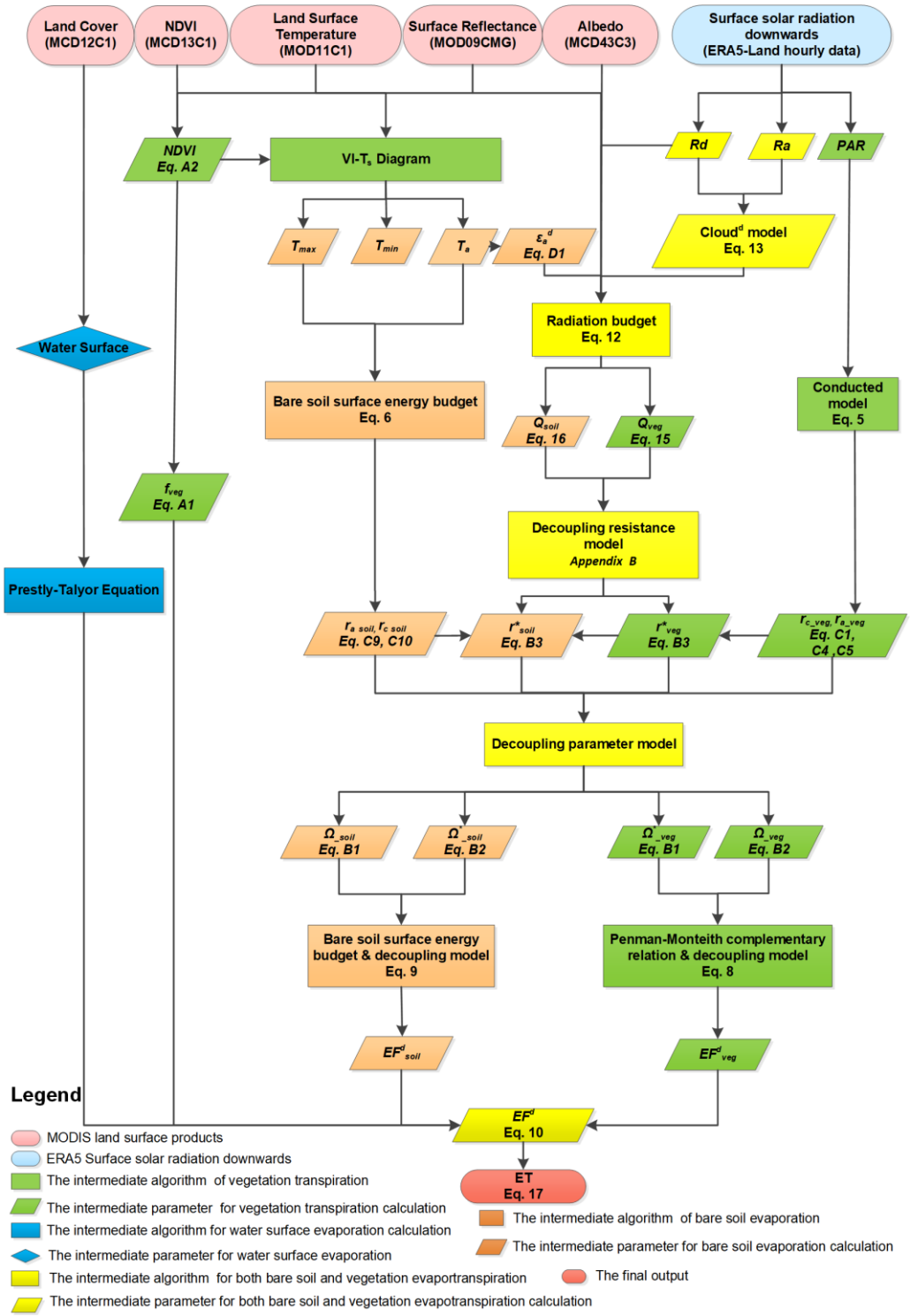

Figure 1. Schematic of VISEA algorithm. The ovals in the top row are the databases, and the square boxes are the algorithms, and parallelograms are the parameters. The numbers in the parenthesis are the equation to determine the parameters.

In our previous studies (Huang et al., 2021 & 2023b), we have continually focused on enhancing the accuracy of the VISEA model, specifically by improving the calculations of daily evaporation fraction and daily net radiation in China. Our current efforts aim to integrate these improvements, expand our study to a global territorial scale, and evaluate VISEA's performance internationally. We are also preparing to publish both the refined algorithms and the global-scale ET data.

Our primary goal is to demonstrate the model reliability on a global scale, and we are committed to ongoing enhancements. Future updates will specifically target reducing biases and further improving the overall performance

L44-46: this claim is problematic since one (i.e. GPCC) is precipitation while another one is ET, so they are difference things even though they have high correlations.

Re: We understand the concern about comparing fundamentally different variables. However, the purpose of this comparison is to validate the spatial distribution of our estimated ET by showing its reasonable correlation with known precipitation patterns. Similar methodologies have been employed in several notable studies, for example: Mu et al., 2007 evaluated the MOD16 data product by comparing precipitation distributions with estimated ET in their Figures 8 and 9 as shown below:

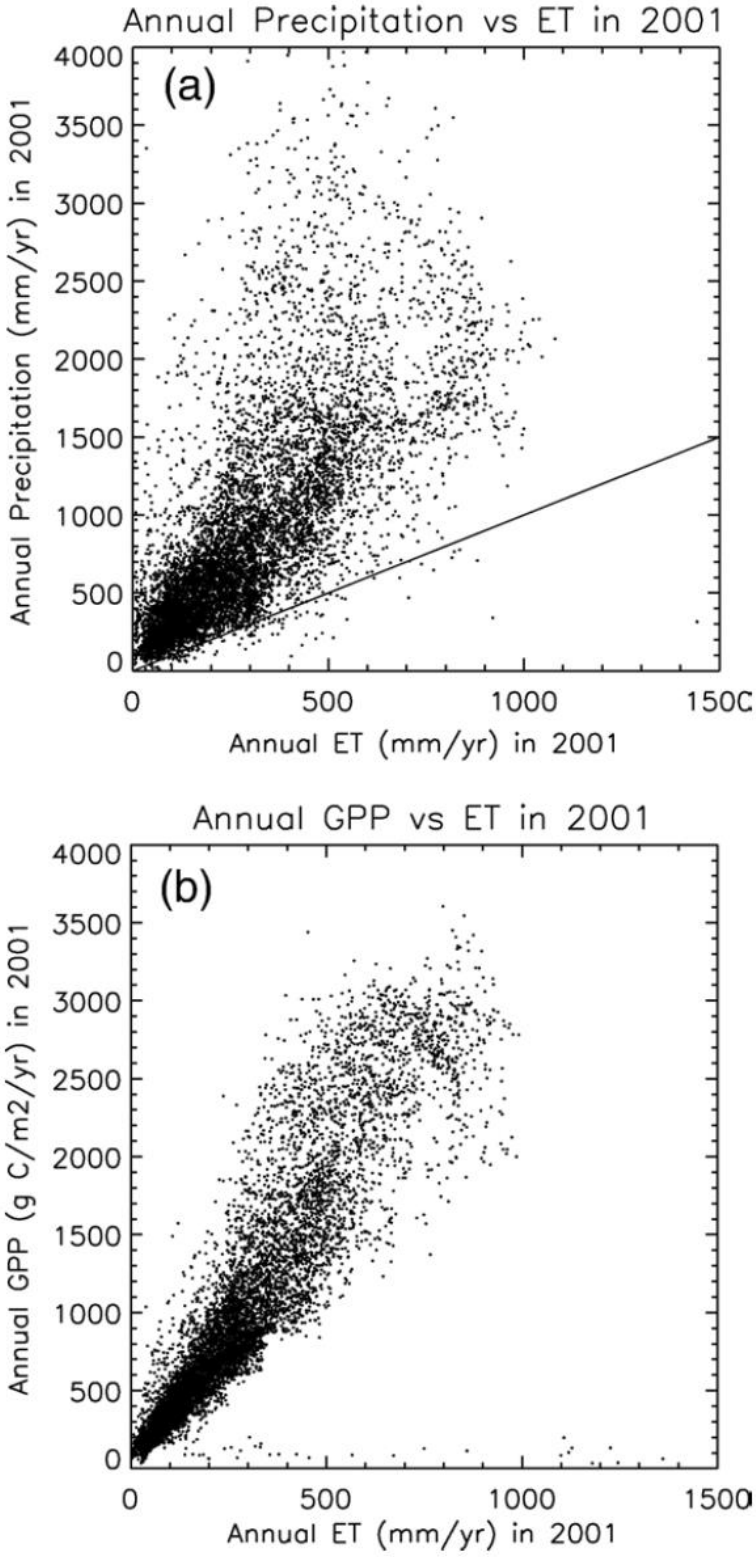

Fig. 8. (a) Annual total precipitation and (b) annual total MODIS GPP versus annual total ET (driven by GMAO meteorological data) in 2001. The solid line in (a) represents that the ratio of ET to precipitation is 1.0.

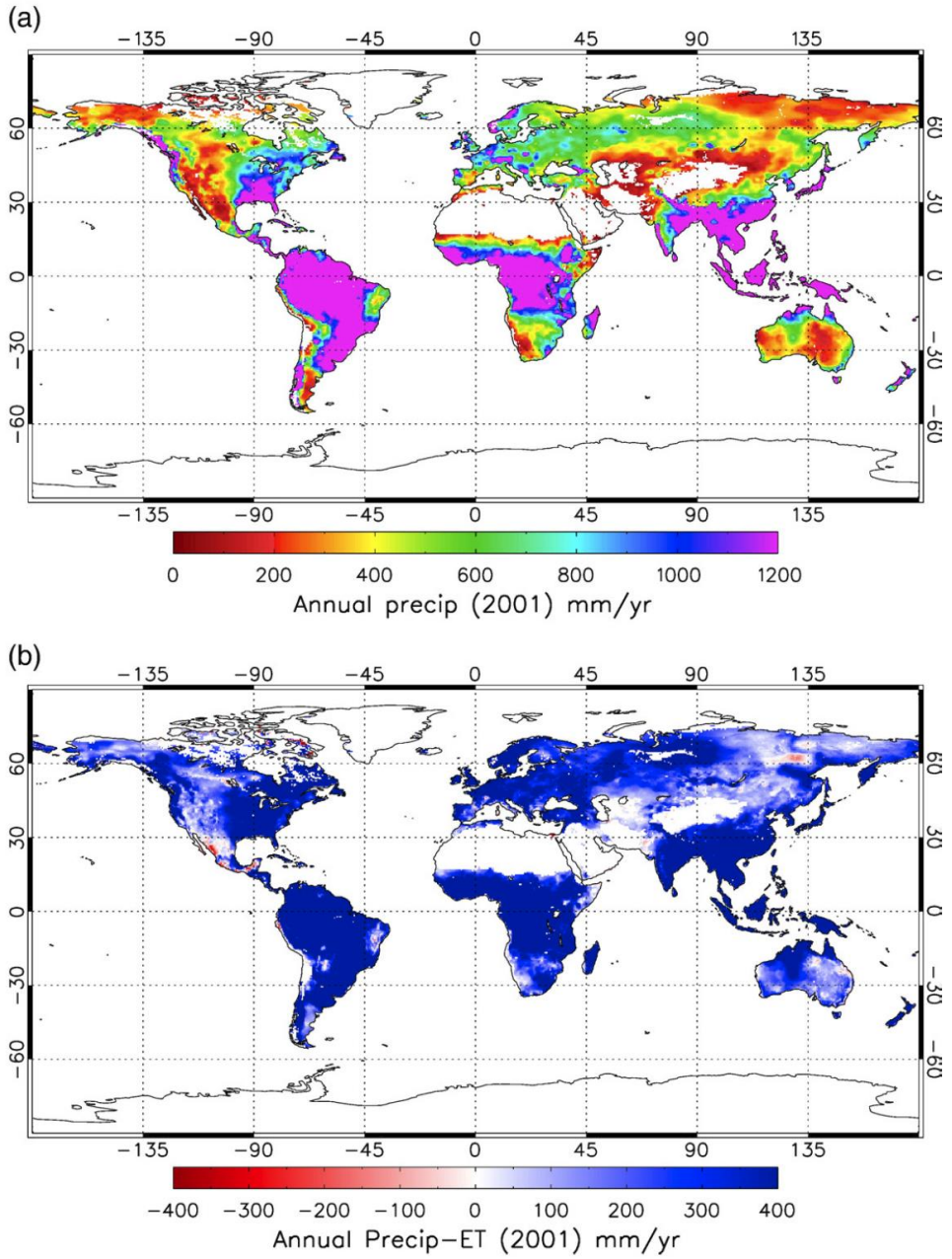

Fig. 9. (a) Global precipitation (precip) in 2001 with a maximum of 7588 mm/yr and an average of 780±686 mm/yr over land. (b) The difference between annual precipitation and annual ET (driven by GMAO meteorological data) in 2001, with a maximum of 4476 mm/yr and an average of 586±568 mm/yr. Vegetated regions are shown in color, and the regions in white are barren or sparsely vegetated areas and non-vegetated areas, including water bodies, snow and ice, and urban areas.

Another example is by Zhang et al., 2019 who compared the distribution of estimated ET and Gross Primary Production (GPP) in their Figure 9.

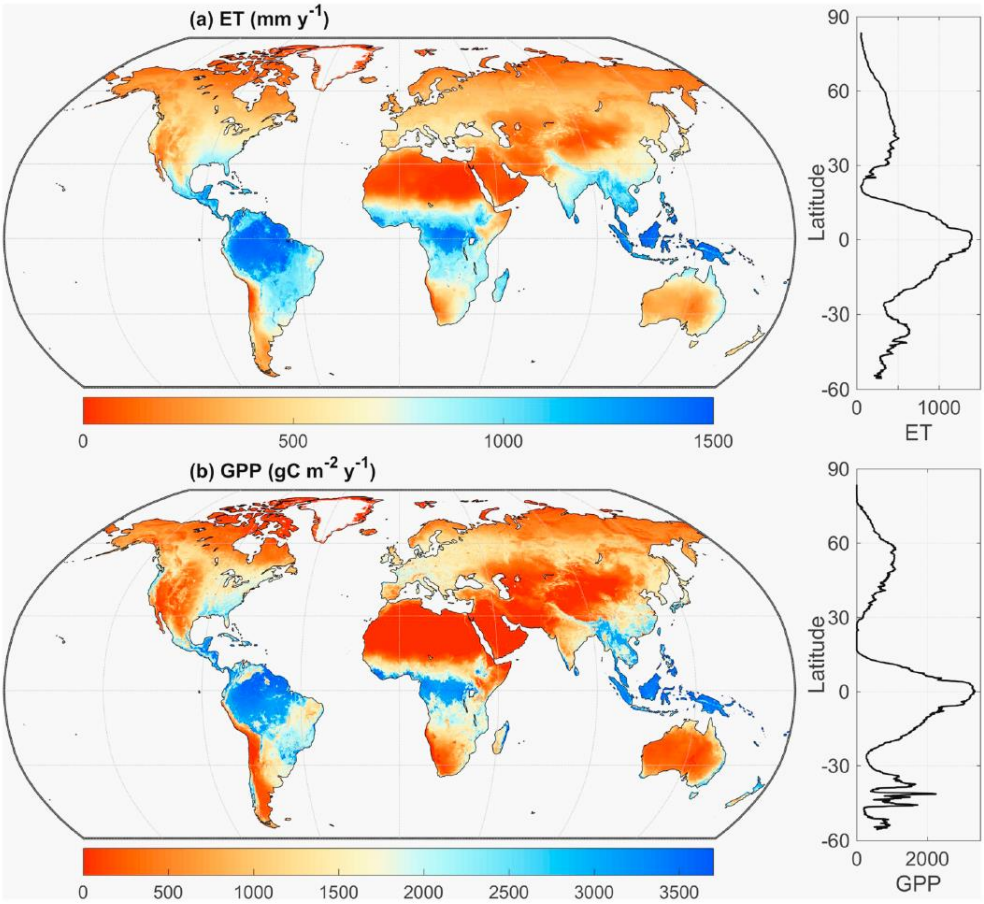

Fig. 9. PML-V2 global average maps of (a) mean annual ET and (b) mean annual GPP for 2003–2017, and their distributions averaged across 1/12° resolution latitudinal bands. These maps are generated at the 1/12° spatial resolution by averaging all 500 m pixels. Water bodies and permanent ice surfaces are excluded for latitudinal averages.

These comparisons demonstrate that the spatial patterns of estimated ET align with other environmental variables and support the validity of the ET estimations.

References:

Mu, Q., Heinsch, F., Zhao, M., and Running, S.: Development of a global evapotranspiration algorithm based on MODIS and global meteorology data, Remote Sensing of Environment, 111, 519–536, https://doi.org/10.1016/J.RSE.2007.04.015, 2007.

Zhang, Y., Kong, D., Gan, R., Chiew, F. H. S., McVicar, T. R., Zhang, Q., and Yang, Y.: Coupled estimation of 500 m and 8-day resolution global evapotranspiration and gross primary production in 2002–2017, Remote Sensing of Environment, 222, 165–182, https://doi.org/10.1016/j.rse.2018.12.031, 2019.

L168: add "temperature" after "air".

Re: We have added temperature after “air” at lines 139-140

In the next section, we will detail how VISEA calculates the daily EF, and Q in Eq. 3, daily air temperature and daily land surface temperature.

The connections between equ. 6 & 7 is not clear, equation B2 might be inserted between these two equations not need explanations.

Re: We have repositioned Equations B1 to B3 between Equations 6 and 7, as they are closely interconnected and provide necessary context for understanding the relationship between these equations at lines 142-156:

Combining Eq. 1, 2 and 3, we calculated the instantaneous evaporation fraction, EF^i as:

$$EF^i = f_{veg}\frac{Q^i_{veg}}{Q^i}\,EF^i_{veg} + (1 - f_{veg})\frac{Q^i_{soil}}{Q^i}\,EF^i_{soil} \quad (4)$$

EF^i_{veg} and EF^i_{soil} are the instantaneous full vegetation coverage and bare soil EF, respectively. EF^i_{veg} can be expressed as a function of instantaneous parameters (Nishida et al., 2003):

$$EF^i_{veg} = \frac{\alpha\,\Delta^i}{\Delta^i + \gamma(1 + r^i_{c\,veg}/2r^i_{a\,veg})} \quad (5)$$

where α is the Priestley-Taylor parameter, which was set to 1.26 for wet surfaces (De Bruin, 1983); Δ^i is the instantaneous slope of the saturated vapor pressure, which is a function of the temperature (Pa K^{-1}); γ is the psychometric constant (Pa K^{-1}); $r^i_{c\,veg}$ is the instantaneous surface resistance of the vegetation canopy (s m^{-1}); $r^i_{a\,veg}$ is the instantaneous aerodynamics resistance of the vegetation canopy (s m^{-1}). EF^i_{soil} was expressed by Nishida et al. (2003) as a function of the instantaneous soil temperature and the available energy based on the energy budget of the bare soil:

$$EF^i_{soil} = \frac{T^i_{soil\,max} - T^i_{soil}}{T^i_{soil\,max} - T^i_a}\frac{Q^i_{soil0}}{Q^i_{soil}} \quad (6)$$

where $T^i_{soil\,max}$ is the instantaneous maximum possible temperature at the surface reached when the land surface is dry (K), T^i_{soil} is the instantaneous temperature of the bare soil (K), T^i_a is the instantaneous air temperature, Q^i_{soil0} is the instantaneous available energy for bare soil when T^i_{soil} is equal to T^i_a (W m^{-2}).

Fig. 8: replace "CPCC" with "GPCC" and suggest add "precipitation" after "GPCC" since only this one is not ET but precipitation.

Re: we have replaced "CPCC" with "GPCC" and added "precipitation" after "GPCC" in Figure 8.

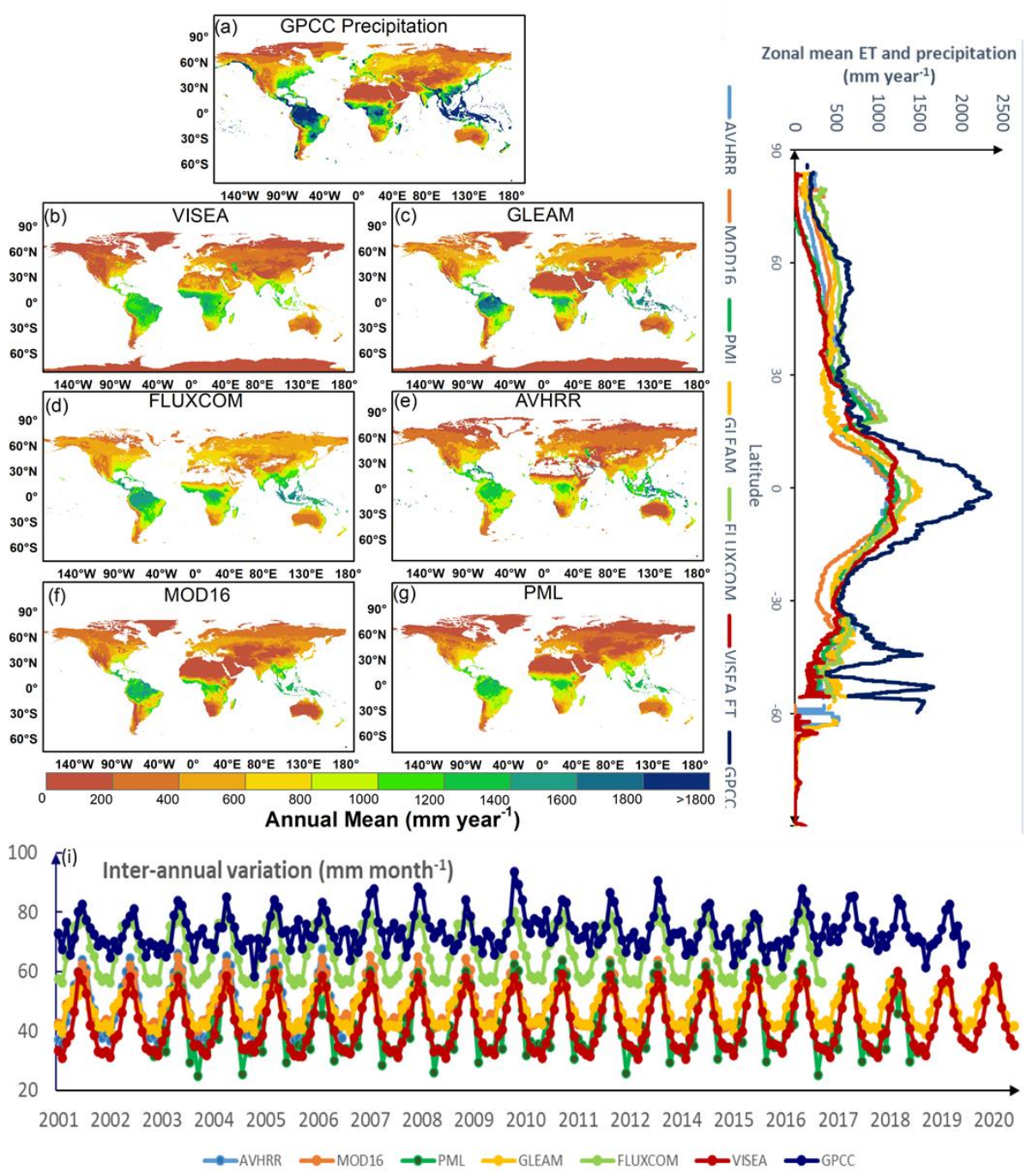

Figure 8. The spatial distribution of the multi-year average (a-g), the zonal mean (h) and inter-annual variation (i) of (a) GPCC precipitation (2001-2019), (b) VISEA (2001-2020), (c) GLEAM (2001-2020), (d) FLUXCOM (2001-2016), (e) AVHRR (2001-2006), (f) MOD16 (2001-2014) and (g) PML (2003-2018) ET data.

L178: incomplete sentence.

Re: We have rewritten this sentence at line 166*:*

According to Pereira (2004), the calculation details of Ω and Ω^* are presented in Appendix B.

Fig.1: the equation numbers are not consistent with the text.

Re: We have corrected the equation numbers of Figure 1.

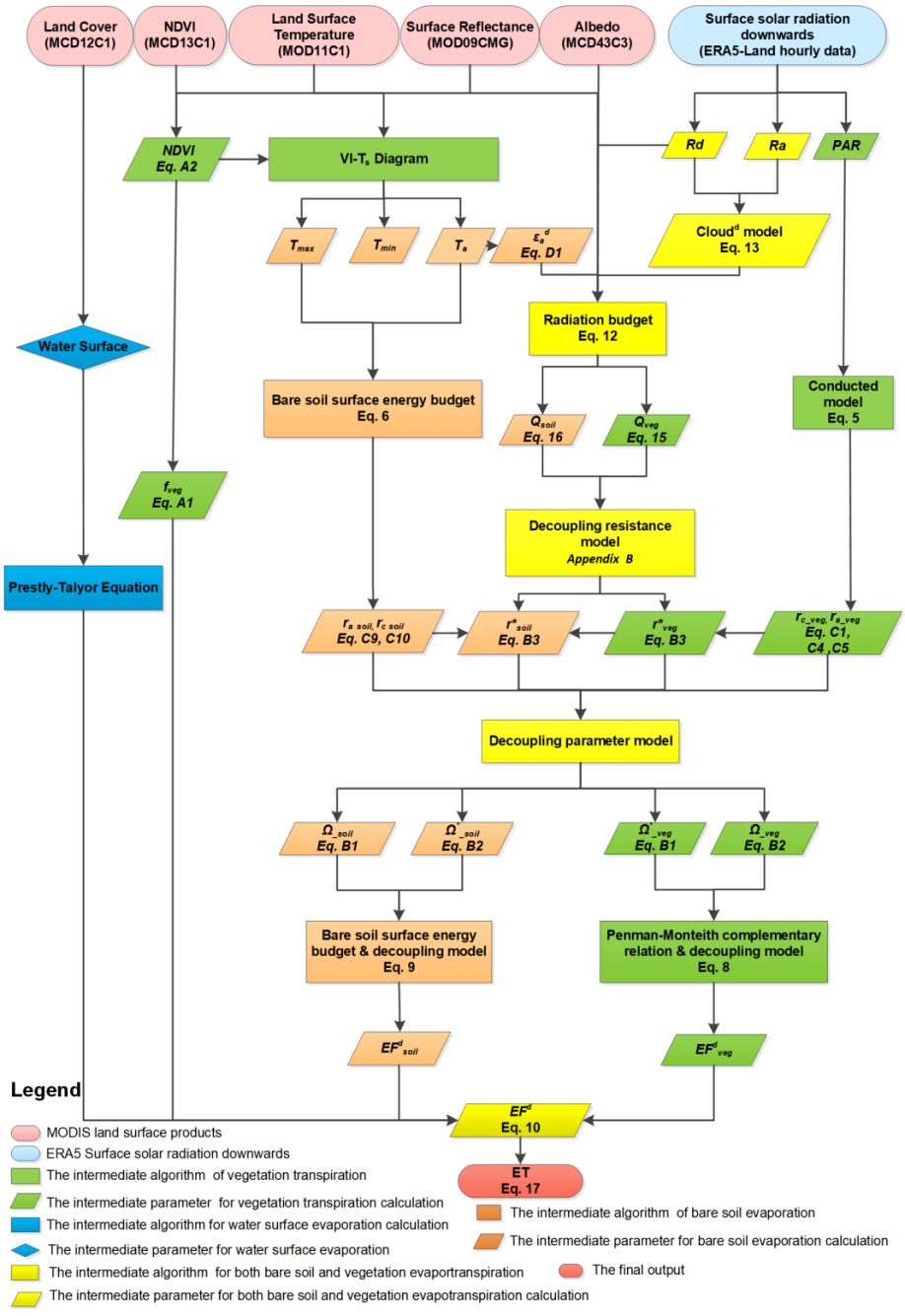

Figure 1. Schematic of VISEA algorithm. The ovals in the top row are the databases, and the square boxes are the algorithms, and parallelograms are the parameters. The numbers in the parenthesis are the equation to determine the parameters.

L185: The "Thus" connection is not clear. Equ. 9: how instantaneous Q, Qsoil and Qveg (and its defination in equ. 8) are calculated?

Re: The sentence has been rewritten as follows at lines 176-178:

The same energy balance equations are used for calculating both instantaneous values Q^i, Q_{veg}^i and Q_{soil}^i and daily values Q^d, Q_{veg}^d and Q_{soil}^d but with parameters adjusted for each timeframe The details of the calculation for the daily values are outlined below.

All equations should be consistent and the name of physical variables should be defined, such as the cloud in equ. 12 and Qsoil 0 .

Re: The definition of $Cloud^d$ in Eq. 15 is added at line 198-200

where $Cloud^d$ is the daily clearness index and K_t is (Chang and Zhang, 2019; Goforth et al., 2002)

$$K_t = \frac{R_d^d}{R_a^d} \tag{14}$$

where R_a^d is the daily extraterrestrial radiation calculated by the FAO (1998).

Q_{soil0}^i is defined at line 156

Q_{soil0}^i is the instantaneous available energy for bare soil when T_{soil}^i is equal to T_a^i (W m^{-2})

L208-210: I don't know what logic is there

Re: These sentences have been rewritten at lines 203-211:

According to the land surface energy budget, the daily available energy of vegetation coverage area, Q_{veg}^d and bare soil Q_{soil}^d can be calculated following the study of Huang et al. (2023b):

$$Q_{veg}^d = \left(1 - albedo^d\right)R_d^d + \ (1 + Cloud^d)\varepsilon_a^d\sigma\ T_a^{d\,4} - \varepsilon_s^d\sigma T_s^{d\,4} \tag{15}$$

$$Q_{soil}^d = (1 - C_G)\left(1 - albedo^d\right)R_d^d + \ (1 + Cloud^d)\varepsilon_a^d\sigma\ T_a^{d\,4} - \varepsilon_s^d\sigma T_s^{d\,4} \tag{16}$$

The daily mean air temperature, T_a^d can be extended by a sin and cos function based on the instantaneous air temperature T_a^i which was calculated using the linear correlation between vegetation index (VI) and surface temperature (Ts) method. Thus, $(1 + Cloud^d)\varepsilon_a^d\sigma\ T_a^{d\,4}$ is the daily downward longwave radiation (W m^{-2}), and $\varepsilon_s^d\sigma T_s^{d\,4}$ is the daily upward longwave radiation (W m^{-2}), where C_G is an empirical coefficient ranging from 0.3 for a wet soil to 0.5 for a dry soil (Idso et al., 1975).

L401-403: the description is vague since Fig. 3 shows comparisons between fluxnet and ERA, nothing related to MODIS products (besides the land cover).

Re: Additional information is provided at lines 390-394:

We chose to utilize 0.05° MODIS data for its detailed land surface information, daily time step, and global coverage, which is essential for accurate and near-real-time ET calculations. Although ERA5 data is at a coarser 0.1° resolution, it provides necessary atmospheric inputs that can be effectively interpolated to match the MODIS resolution without significant loss of accuracy. As illustrated in Figures 3 and 4, our tests confirm that this method achieves accurate ET despite the resolution differences.

L554-590: most of the results are not new and should avoid to say which model "overestimate" or "underestimate" without compare with the ground truth.

Re: we have rewritten these paragraphs at lines 564-600:

The VISEA ET product demonstrates consistent spatial distribution patterns among the six ET products across various years in terms of annual means (a-g) and latitude zonal means (h). These patterns closely align with the precipitation distribution data from GPCC. Furthermore, VISEA ET also exhibit similar spatial distributions compared to other ET products, particularly in the extremes of the distribution, below the 5^{th} percentile and above the 95^{th} percentile (Figure S6, S7). The highest ET values, approximately 1,500 mm $year^{-1}$, are predominantly in equatorial low-latitude regions with the corresponding high precipitation levels of approximately 2,500 mm $year^{-1}$. These regions include South America (Amazon Basin), Central Africa (Congo Basin), and Southeast Asia (encompassing Indonesia, Malaysia, parts of Thailand, and the Philippines), which have tropical rainforest climates. Remote sensing data support the ET estimates and align with findings from previous studies, such as Chen et al. (2021) and Zhang et al. (2019), who reported that the multi-year average annual ET is nearly 1,500 and the precipitation is approximately 2,500 mm $year^{-1}$. Also, Panagos et al. (2017) report similar multi-year average annual ET and precipitation rates.

In this analysis, barren lands (BAR) such as the Sahara, Arabian, Gobi, and Kalahari deserts, along with large areas of Australia, and snow and ice (SI) regions including significant parts of Canada, Russia, and the Qinghai-Tibet Plateau in China, are characterized by notably low evapotranspiration (ET). These regions typically experience less than 400 mm $year^{-1}$ of annual ET, paralleled by minimal yearly precipitation ranging from 200 to 400 mm $year^{-1}$, according to GPCC data. Comparative ET rates for other land cover types generally range from 400 to 1,400 mm $year^{-1}$, closely following the GPCC precipitation amounts of 600 to 1,600 mm $year^{-1}$.

In regions experiencing moisture-limited evapotranspiration (ET), the scarcity of available water is the primary constraint. Conversely, in areas where sufficient water is available, ET is energy-limited, and factors such as cloud cover or shading restrict the absorption of solar radiation, affecting the evapotranspiration rate. Panel (i) in Figure 8 illustrates inter-annual monthly variations over the past two decades. It shows how VISEA and other satellite-based ET products, alongside GPCC precipitation data, capture the rhythmic patterns of ET. These data reveal distinctive seasonal fluctuations and highlight the significant inter-annual climate variability. Among these products, FLUXCOM consistently shows ET values 10-20 mm month^{-1} higher than those of other ET products. GLEAM and MOD16 exhibit similar ET estimations, closely paralleling each other, as do PML and VISEA. Notably, after 2007, both GLEAM and MOD16 reported higher ET estimations than PML and VISEA in November, December, January, and February. For the same months, PML consistently records lower ET estimations than VISEA.

Analysis across the datasets reveals how ET estimates respond to extreme climate events, providing insights into the variability and resilience of these models. For instance, during the 2011-2012 drought in the Horn of Africa—one of the most severe droughts in recent decades—both ET estimations and GPCC precipitation data showed significant declines. Similarly, the prolonged California drought from 2012 to 2016 also saw a considerable decrease in ET values, aligning with the reduced precipitation levels captured by GPCC.

Fig.8: need dig into more details on the differences in long-term trends and the variations in the years with extreme climate events.

Re: we have added more details on the differences in long-term trends and the variations in the years with extreme climate events at lines 590-600:

Among these products, FLUXCOM consistently shows ET values 10-20 mm month^{-1} higher than those of other ET products. GLEAM and MOD16 exhibit similar ET estimations, closely paralleling each other, as do PML and VISEA. Notably, after 2007, both GLEAM and MOD16 reported higher ET estimations than PML and VISEA in November, December, January, and February. For the same months, PML consistently records lower ET estimations than VISEA.

Analysis across the datasets reveals how ET estimates respond to extreme climate events, providing insights into the variability and resilience of these models. For instance, during the 2011-2012 drought in the Horn of Africa—one of the most severe droughts in recent decades—both ET estimations and GPCC precipitation data showed significant declines. Similarly, the prolonged California drought from 2012 to

2016 also saw a considerable decrease in ET values, aligning with the reduced precipitation levels captured by GPCC.

L591-612: the arguments are statistical weak and the mismatch of spatial (and temporal) pattern between VISEA and precipitation can not support the conclusion that VISEA is better than another model. Authors need discuss the effects of soil moisture on ET, besides the precipitation events.

Re: This part is modified by adding a discussion on the effects of soil moisture on ET, besides the precipitation events at lines 609-629:

Figure 9 presents the daily ET from VISEA and GLEAM, alongside precipitation data from the GPCC across the Yangtze River Basin from August 26th to September 2nd, 2022. During this period, a significant drought was observed in the region, which began in July and showed signs of abating by late August and early September, according to Zhang et al. (2023). VISEA ET illustrates the evolving drought conditions, with notably low ET levels (below 1 mm day^{-1}) across the basin from August 26th to 28th, as shown in panels (a-c). A marked increase in precipitation on August 29th, evident in panels (s) and (u), correlates with an uptick in ET values (surpassing 1 mm day^{-1}) throughout the basin, visualized in panels (d-f). Although GLEAM generally captures the fluctuations in ET—both decreases and increases—during this period, it consistently reports much higher ET values than VISEA. The panel (y) graph in Figure 9 shows the precipitation and the ET calculated by VISAE and GLEAM after an 11 mm rainfall on August 29th. The ET of VISEA increased and the deceased, which is expected because ET and soil moisture are positively correlated. The GLEAM does not follow the expected pattern shown in panel y. This comprehensive analysis highlights the interdependence of precipitation and ET and underscores the importance of considering soil moisture dynamics to fully understand the hydrological processes within the Yangtze River Basin during extreme weather events.

Beyond precipitation, soil moisture is a critical regulator of ET, particularly during droughts and their recovery phases. Acting as a buffer, soil moisture tempers ET rates during dry periods and amplifies them after rainfall, as noted in late August. This buffering capacity results in a delay between precipitation events and subsequent ET changes, which is key to understanding drought recovery dynamics. VISEA's data accurately reflect these variations in precipitation, demonstrating its effectiveness in tracking daily ET fluctuations and its reliability for near-real-time monitoring of ET during hydrological extremes.

L630-631: rephrase since it mixed the information from observations (shortwave downwards radiation) and estimated variables such as air temperature (pixel scale).

Re: we have rewritten this sentence at lines 647-650:

The VISEA model uses gridded ERA5-Land shortwave downward radiation as its energy input. Utilizing this input, along with MODIS land surface products, VISEA calculates gridded daily air temperature and net radiation. These two important intermediate variables are essential for estimating daily ET.

L653-655: incomplete sentence.

we have rewritten this sentence at lines 668-670:

As previously explained, the VI-Ts method relies on the negative linear correlation between the Vegetation Index (VI) and surface temperature (Ts) within a 5 × 5 grids' window. Therefore, both the variance of VI values across these grid cells and the strength of their negative correlation are crucial for accurately calculating air temperature.

L655-657: unclear.

Re: we have rewritten this sentence at lines 668-676:

As previously explained, the VI-Ts method relies on the negative linear correlation between the Vegetation Index (VI) and surface temperature (Ts) within a 5 × 5 grids' window. Therefore, the variance of VI values across these grid cells and the strength of their negative correlation are crucial for accurately calculating air temperature (Nishida et al., 2003). However, the VI-Ts method is less effective in regions like dense forests, bare lands and deserts, where the vegetation index and temperature data vary little across the 5 × 5 grids' window. Also, in regions with freezing temperatures, the VI-T_S method does not perform well because warmer temperature is related to increased vegetation, which is the opposite of warmer areas, where there is a positive correlation between the vegetation index and surface temperature (Cui et al., 2021).

L691-693: The logic is not clear. Does it mean this model can only be used from 60N-90N?

Re: we have rewritten this sentence at lines 696-710:

While the VISEA model provides evapotranspiration (ET) globally, its best ET is between 60°N and 90°S, as evidenced by a Nash-Sutcliffe efficiency (NSE) of 0.4 and a correlation coefficient (R) of 0.9 in Figure 6. VISEA model tends to underestimate ET in colder regions within the 60°N to 90°S latitude range, such as the western territories of Canada. This underestimation is primarily due to the model's inability to

incorporate evaporation from frozen surfaces into its ET calculations. These discrepancies arise from several factors: inaccuracies in the ERA5-Land shortwave radiation data (illustrated in Figure 3), the misapplication of the VI-Ts method (explained in Figure 4), and the uncertainties in daily net radiation (depicted in Figure 5). Designed to amalgamate bare soil and full vegetation coverage, as shown in Equation 1, the VISEA model encounters difficulties in accurately estimating ET at higher latitudes, especially in conditions of reduced solar radiation. These challenges are predominantly linked to the uncertainties associated with ERA5-Land shortwave radiation data, further compounded by increased cloudiness levels in these regions, as highlighted by Babar et al. (2019). Such uncertainties substantially impact the model's performance at higher latitudes, affecting its reliability in these conditions. Nevertheless, VISEA's ET estimates compare favorably with other ET data products in cold regions above 60°N, as indicated by the latitude zonal mean comparison in Figure 8.

L843-845: it's still very strange to claim that VPD and leaf water potential "can be omitted" from the calculation of canopy resistant. Which factor could affect stomata conductance then?

Re: we have rewritten this sentence at lines 828-836:

In this study, we follow the methodologies originally developed by Tang et al. (2009) and Nishida (2003), with the goal of enhancing the VISEA model to accurately estimate daily scale evaporation fraction and net radiation. These efforts build on earlier work by Huang et al. (2017, 2021, and 2023b) that introduced vapor pressure deficit (VPD) and leaf water potential in calculating canopy resistance. However, comparative analyses between VISEA and other models, such as PML and MOD16—particularly PML, which integrates VPD as a limiting factor in estimating GPP and ET—show that VISEA maintains accuracy without significant biases. It is important to note that none of the ET models in our comparison directly incorporate leaf water potential into their canopy resistance calculations. We are committed to addressing these gaps in our future studies.